Metal Organic Framework based PVDF-Separators for High Rate Cycling Lithium-Ion Batteries

Ainara Valverde[a], Renato Gonçalves[b], María M. Silva[b], Stefan Wuttke[a,c], Arkaitz Fidalgo[a,d], Carlos M. Costa[b,e*], José L. Vilas-Vilela[a,f], José M. Laza[f], María I. Arriortua[a,g], Senentxu Lanceros-Méndez[a,c], Roberto Fernández de Luis[a*]

[a]BCMaterials (Basque Centre for Materials, Applications & Nanostructures), Bld. Martina Casiano, 3rd. Floor UPV/EHU Science Park Barrio Sarriena s/n 48940 Leioa, Spain

[b]Centre of Chemistry, University of Minho, 4710-057 Braga, Portugal

[c]IKERBASQUE, Basque Foundation for Science, 48013 Bilbao, Spain

[d]Dept. of Organic Chemistry II, University of the Basque Country (UPV/EHU), Barrio Sarriena s/n, Leioa, Bizkaia 48940, Spain

[e]Centre of Physics, University of Minho, 4710-057 Braga, Portugal

[f]Macromolecular Chemistry Group (LABQUIMAC), Department of Physical Chemistry Faculty of Science and Technology, University of the Basque Country (UPV/EHU), Barrio Sarriena s/n 48940 Leioa, Spain, 48013 Bilbao, Spain

[g]Mineralogy and Petrology Department, Faculty of Science and Technology, University of the Basque Country (UPV/EHU), Barrio Sarriena s/n 48940 Leioa, Spain, 48013 Bilbao, Spain

KEYWORDS: Separator membranes, MOF-808; PVDF; separator; lithium-ion battery

---

* **Corresponding Authors**

Carlos M. Costa (cmscosta@fisica.uminho.pt),

Roberto Fernández de Luis (roberto.fernandez@bcmaterials.net)

ABSTRACT: Poly(vinylidene fluoride) (PVDF) and MOF-808 based separators for lithium-ion batteries (LIBs) have been prepared and fully characterized in terms of morphological and thermal properties, electrolyte uptake and retention, and surface hydrophilic characteristics. The effect of PVDF/MOF-808 separators on the electrochemical performance of LIBs has been evaluated. The PVDF/MOF-808 membranes exhibit well-defined porous structure with a uniform distribution of interconnected macro- to mesopores. The inclusion of the Zr-based MOF increases the porosity and surface area of the separator and enhancing the electrolyte uptake and the ionic conductivity. Finally, the presence of MOF-808 fillers improves the liquid electrolyte retention, which prevents the capacity fading at high C-rates cycling. Indeed, charge-discharge tests performed in Li/C-$LiFePO_4$ half-cells reveal a discharge capacity of 68 $mAh.g^{-1}$ at 2C-rate for PVDF/MOF-808 membranes, in comparison with the 0 $mAh.g^{-1}$ obtained for pure PVDF. The PVDF/10 wt% MOF-808 sample shows a long-term stable cycling behaviour with a coulombic efficiency close to 100%. Thus, it is shown that the composite membranes represent an improvement with respect to conventional separators for lithium ion battery applications, since they coupled the polymer meso and macro porous structure with the well-ordered microporous system of the MOFs, which improve significantly the electrolyte affinity.

1. INTRODUCTION

The increasing impact of fossil fuels on global warming leads to the need of a transition to an economic system based on green energy[1-2]. Currently, lithium ion batteries (LIBs) are so far the best commercially available energy storage solution. Nevertheless, LIBs still show key drawbacks to be solved, such as their high production costs and capacity fading during operation at high charge and discharge rates. [3]

LIBs are build-up by positive and negative electrode components, which are electronically isolated by a porous polymeric separator wetted in liquid electrolyte [4]. Until recently, the research community has paid less attention to the characteristics of the battery separators, considering them a passive element of LIBs. Nevertheless, it has been duly demonstrated that the separator is an essential active barrier that strongly affects the fast, reversible and long-term stable ionic transport in LIBs during operation[5,6].

Ionic migration through the separator is not directly related to the value of the ionic conductivity of the separator-electrolyte system. Effective Li^+ migration only occurs for a portion of total ionic conductivity, and it is highly dependent on the porous structure [7] (*e.g. degree of porosity (%) [8-9] tortuosity or heterogeneity [10]*), and the surface interaction between the liquid electrolyte and the separator matrix (*e.g. liquid electrolyte uptake (%), wettability (contact angle)…*)[11]. Therefore, the interplay between a highly interconnected porous structure and the proper surface to electrolyte interaction will shape the facile and fast ionic mobility paths through the separator [12-13].

Most commercially available LIB separators are build up from polyolefin membranes based on either semi-crystalline polyethylene (PE) and/or polypropylene (PP), showing total po-

rosity ranging from 40-80 %, and thickness varying from 25 to 50 microns [14-15]. These commercial membranes present drawbacks such poor wettability and thermal stability and high flammability. In order to modify their surface chemistry and, specifically, their wettability by the electrolyte, inorganic nanoparticles (e.g. Al_2O_3 [16], SiO_2 [17], TiO_2 [18], $Al(OH)_3$, $Mg(OH)_2$ [19] and ZrO_2 [20-23]) are being used as active fillers and layers on polymer based separators. These composite membranes have shown improved ionic conductivity and wettability together with long cycling stability under working conditions.

In this work we have selected Metal-Organic Frameworks (MOFs) as novel porous fillers[24-26] and highly mechanical, thermal and chemical resistant poly(vinylidene fluoride) (PVDF) as polymer matrix to develop novel battery separator membranes.

PVDF based separators have an excellent chemical and mechanical stability in comparison to commercial PE and PP systems. In addition, PVDF can be easily processed[27] as anisotropic porous separator membranes; which structure consists on a dense skin layer accompanied by finger-like and sponge-like channels (Scheme 1a). This PVDF structure was selected for two reasons: 1) the sponge-like region endows the separator of a highly interconnected porous structure while 2) the dense but porous skin layer is foreseen to allow the lithium ions migration while acting as a barrier for lithium dendrites growth.

MOFs, and specifically highly chemically stable Zr(VI) based MOFs, offer multiple advantages as active fillers for separators in comparison with inorganic ceramics. Specifically, among the large variety of Zr-based MOFs synthesized up to date, MOF-808 was selected because it exhibits a highly ordered and chemical tunable meso-porous structure (*i.e. pore diameter ~ 18 Å, surface areas over* m^2/g [28-32]) that can act as a liquid electrolyte reservoir. In addition, MOF-808 particle size and morphology can be easily controlled down to the

nanometer scale, since nano-fillers can play an important role as modulators of the meso and macro-porous structure of the polymeric support during its processing. Finally, the presence of acid positions at the $Zr_6O_4(OH)_{4+x}(H_2O)_{2x}(\text{-}COO)_{12-x}$ hexa-nuclear clusters that forms the MOF-808 structure is also an important aspect to consider, since it has been recently proved to be highly beneficial to enhance the lithium transfer paths through the separators[33].

All the above-mentioned characteristics play an important role to influence the PVDF/MOF separator porous structure and surface chemistry from the macro to the angstrom scale (illustrated in Scheme 1). At the macroscopic scale, the dispersion of MOF nanoparticles inside the PVDF solution will modulate the porous structure of PVDF during its processing. The straightforward control of the MOF fillers loading in PVDF membrane enables to tune the overall porosity, homogeneity, shape and size of the macro/mesoporous structure of the PVDF polymeric membrane (Scheme 1 a) [34-36]. At the nano-metric scale, the surface chemistry of the MOF nanoparticles is composed of under coordinated zirconium clusters and organic linkers that can act as interacting points for the anionic and cationic species found in the electrolyte. Hence, the surface of the MOF nanoparticles could be understood as docking and transport points for lithium during its migration (Scheme 1b) [37-39]. Last but not least, at the angstrom scale, the porous MOF structure itself can act as an extra electrolyte storage space. In addition, the MOFs pores can also act as ion carriers, since MOFs usually exhibit two to three order of magnitude enhancement of their ionic conduction after soaking them in liquid electrolytes or ionic liquids (Scheme 1c) [40].

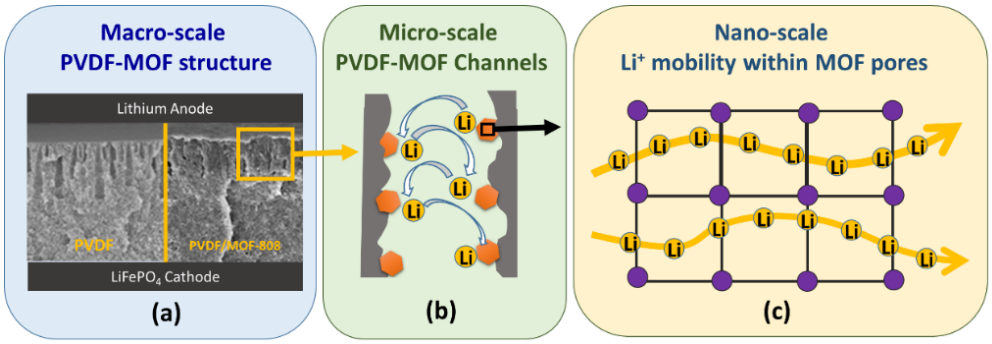

Scheme 1. Illustrative pictures of PVDF/MOF-808 composite structures at (a) macro, (b) meso and micrometric and (c) nano-Armstrong scales. The role of (b) MOF nanoparticles and (c) MOF´s inorganic clusters within the porous structure as ion mobility enhancers through the anions docking points have been also represented.

Despite MOF materials are relatively expensive in comparison to classic PP or PE polymeric separators used in LIBs, several studies point that MOFs have a beneficial role as components for separators of Lithium Sulphur, Lithium air and Lithium ion batteries; leading to an increase in the long term stability of the cell over cycling [41-43].

Nevertheless, none of the previous works has determined the effect of the MOF nanoparticle fillers as modulators of the macro and mesoporous structure of the separator, relating them with the electrochemical performance of the battery. In this study, we have investigated MOF-808 nanoparticles loading on the PVDF separators porous structure, surface properties, electrochemical performance and stability over cycling. It is worthy to mention that the potential of MOF based separators are large, since the chemistry and properties of the MOF fillers can be tuned even after they are incorporated in the polymeric matrix, Therefore, once identified the best characteristics of the MOF/polymer composite, which is the main aim of this work, the chemical nature of the membrane – liquid electrolyte interface can be tailored

through the post-synthetic chemical encoding of Zr based MOF fillers. Also, we selected $LiFePO_4$ as active material to test the battery performance of the new separators due to its excellent properties, that include low density (3.6 g/cm^3) and a high theoretical capacity of 170 mAh/g (2.0 -4.0 V)

2. EXPERIMENTAL

2.1. Materials

N,N-Dimethylformamide (DMF) (purity 99.9%) and formic acid (purity 98%) were obtained from Labkem. $ZrCl_4$ (purity 99.3%) was purchased from Alfa Aesar, and Trimesic acid was supplied from Sigma Aldrich. PVDF (Solef® 1010 and Solef® 5130) were purchased from Solvay. C-$LiFePO_4$ (LFP), carbon black (Super P-C45), N,N'-dimethylpropyleneurea (DMPU) and the electrolyte 1M $LiPF_6$ in ethylene carbonate-dimethyl carbonate (EC-DMC, 1:1 vol) were acquired from Phostech Lithium, Timcal Graphite & Carbon, LaborSpirit and Solvionic, respectively.

2.2. MOF-808 synthesis

$ZrCl_4$ (0.3084 g, 0.33075 mmol) was dissolved in a DMF solution (30 mL). Then formic acid (30 mL, 1.985 mmol) and trimesic acid (0.3092 g, 0.3675 mmol) were added. Finally, of distilled water (1.25 mL) was added to the reaction media as modulator agent. The mixture was kept at 120 ºC for 24 hours in a screw-capped glass jar (100 mL), and then washed several times with DMF. After the synthesis, the sample was thoroughly washed with DMF three times until a dispersion of MOF-808 particles of known concentration (20 mg/L) was obtained. Drying and activation step of the MOF-808 materials were avoided in order to

prevent/diminish the particle agglomeration during the membrane preparation. The synthesis can be easily scaled to higher volume reactors (500 mL), but instead of 24 h, the reaction time was increased to 48 h to assure the complete crystallization.

2.3. PVDF/MOF-808 membrane preparation.

The PVDF/MOF-808 membranes were prepared following the Non-solvent Induced Phase Separation (NIPS) procedure suggested by Ribeiro et al.[27]. Solution A: 15mL PVDF 1010 solution (30% wt) was prepared using DMF as the solvent. Solution B: 15mL of MOF-808/DMF dispersions was prepared. The concentration of the MOF-808 nanoparticles in the different dispersions was calculated to obtain a 5 %, 10 % and 15 % weight percentage of the MOF-808 with respect to the PVDF dissolved in the solution A. Afterwards, solution B was added to the solution A under ultrasonication during 10 min. The solution was then spread on a glass substrate using a doctor blade, obtaining a film of 250 μm. After casting the solution onto the glass substrate plates, the assembly was immediately immersed in a distilled water coagulation bath at 60 ºC. After 30 minutes in the bath, the film was removed and immersed in a distilled water bath at room temperature, in order to remove possible traces of solvent. Finally, the film was allowed to air-dry at room temperature during 24 hours.

2.4. Characterization techniques.

The X-ray diffraction pattern of MOF nanoparticles and CH/MOF-808 composites were obtained in a Panalytical X´pert CuKα diffractometer 2θ range = 5–70°, step size = 0.015°, exposure time = 10 s per step at room temperature. Panalytical X´pert is a polycrystalline sample diffractometer with theta-theta geometry, a programmable slit, secondary graphite

monochromator adjusted to a copper radiation and fast solid state PixCel detector adjusted to an 3.347º active length in 2θ(º). The equipment allows to perform quality measurements for the subsequent data processing, at the level of full profile adjustments without/with a structural model. XRD data of MOF-808 particles synthesized following the initial method reported by J. Jiang. et. al. [44] (Figure S1a) as well as the MOF-808 nanoparticles obtained through water-modulator approach (see above), were fitted by a profile matching analyses in order to confirm the purity of the samples (Figure S1b). X-ray diffraction patterns of the PVDF/MOF-808 membranes were fitted with a multiphase Rietveld analyses containing the structural models for PVDF α and β phases, in addition to the MOF-808 structural model. Rietveld analyses allow quantifying the MOF-808 loading, as well as the PVDF alpha/beta ratios in membranes with different MOF-808 contents. Simulated X-ray diffraction (XRD) patterns of β and γ PVDF polymorphs are quite similar in the low 2θ (º) region, where most of the information of the experimental XRD patterns is located [45]. This makes difficult to differentiate the β and γ PVDF polymorphs by XRD experimental data. Structural models of the different phases taken into account during the refinement were not modified. The scale factors obtained after the refinement were used to calculate the weight percentage of the phases in the PVDF/MOF-808 composites. The semi-quantification of the MOF-808 in the PVDF matrix was determined performing a two phases Rietveld analysis with the structural models of the α-polymorph of PVDF and MOF-808. During the refinement, the fitting of the profile and cell parameters for all phases was carried out until convergence. It is worthy to notice that it was necessary to refine the background to obtain a final reasonable fit of the experimental data. The background intensity and shape can account for the amorphous part of the PVDF matrix.

Once reached this point in the refinement, the experimental data of the most intense 2θ region between 12-25º still show some degree of mismatching with the Rietveld simulated data. Therefore, it was considered the contribution of the β-polymorph of PVDF in the refinement, obtaining as a result a significant improvement of the agreement factors. Figure S2 shows the final fittings, as well as the contributions to the experimental data coming from the PVDF polymorphs, MOF-808 and background. It is important to point out that even when the experimental fittings indicate the α and β-polymorph qualitatively, the absolute quantification values need to be interpreted carefully. Figure S1a-b and S2 show the pattern matching and Rietveld analyses fit for the different MOF-808 samples and PVDF/MOF-808 membranes, respectively.

The morphology of the MOF-808 nanoparticles was observed by transmission electron microscopy (TEM), using a Philips Supertwin CM200 transmission microscope operated at 200 kV and equipped with a LaB6 filament and EDAX-DX-4 microanalysis system. The equipment incorporates double tilting sample holder, an Megaview III rapid acquisition camera, and a high resolution (4K x 4K) and high sensitivity digital camera. MOF-808 nanoparticles were previously dispersed in ethanol by applying ultra-sonication during 10 min. The nanoparticle suspension was dropped on a copper grid placed on the sample holder and was dried under vaccum for 15 min. overnight. Before introducing the samples into the microscope, they were thoroughly dried under ultra-vacuum during 15 min.

Morphology of the PVDF/MOF-808 membranes was evaluated by Scanning Electron Microscopy (SEM), SEM of Schottky field emission (JEOL JSM-7000F) microscope has resolution in secondary electrons of 1.2 nm at 3KV and 3 nm at 1 KV; and a 3nm resolution with

electron backscattered to 15 KV and 10 mm working distance. The accelerating voltage is variable between 0.5KV and 30KV and the beam current is 1 PicoA and 200nA.

Nitrogen sorption isotherms were measured at 77 K with a Quantachrome Autosorb-iQ-MP and at 273K with a Quantachrome ISorb instruments. Approximately 10 - 20 mg of MOF NPs was degassed at 120 C in high vacuum for at least 12 h prior to the measurement. Porosimetry of PVDF/MOF-808 composites were determined by mercury intrusion porosimetry (MIP) in a Quantachrome Instruments Poremaster-60 GT operating in the pressure range from vacuum (10-4 MPa) to 414 MPa. Samples were degassed in situ at 110 ºC during 12 h prior to measurement. A contact angle of 140º and a surface tension of 480 dyn•cm-1 for mercury and a pressure equilibration time of 11 s were used. Before the measurement of MIP the He density for all the samples were measured in a Quantachrome Instruments automatic Micro Ultrapycnometer. The surface area values were obtained by the fittings of the adsorption data to a linearized for of the Brunauer–Emmett–Teller (BET) equation. For all samples the correlation coefficient was higher than 0.999.

Thermogravimetric analyses were carried out with a Shimadzu thermobalance, model DTG60 (Columbia, USA), under dynamic air atmosphere (20 mL min^{-1}). An alumina crucible containing ca. 25 mg of the sample was heated at 5 °C min–1 in the temperature range 30–700°C.

Difference Scanning Calorimetric (DSC) analyses were performed on Mettler-Toledo DSC 822e (Gießen, Germany) under heating-cooling-heating cycles from -100 to 200 ºC, down to -100 ºC and finally back up to 200 ºC. Measurements were performed under N2 atmosphere (flow rate 50mL/min) in aluminum pans with a sample weight 7 to 10 mg. The data for the first heating ramp has been discussed in the manuscript, whereas the second heating ramp

has been used to assess the reversibility of the processes observed in the first ramp. The heating rate was 10K/min, whereas the cooling rate was 20 K/min. The heating ramps of the experiments were the relevant sections of the DSC measurement that allow determining the MOF-808 loading, follow its de-hydration process and determine its reversibility. The velocity of the cooling rate was increased in order to acquire the complete data faster.

Fourier-transform infrared spectroscopy (FTIR) spectra measurements were carried out using a Jasco FT/IR-6100 spectrometer in Attenuated Total Reflectance mode (FTIR-ATR). Each spectra were recorded from 600 to 4000 cm^{-1} wavelengths with a 1 cm^{-1} resolution. 64 scans were measured and averaged to obtain the final spectra.

The contact angle of the samples was measured with an optical system Dataphysics OCA 15EC Neurtek Instrument. Drops of Milli-Q water were dropped on each sample (2 μL/drop) and three measurements per sample were carried out in different sample locations.

2.5. Uptake and ionic conductivity determination

The membranes were immersed in the liquid electrolyte, consisting in a 1 M solution of $LiPF_6$ in EC-DMC, 1:1 vol, for 15 minutes and the uptake was calculated by equation 1:

$$\varepsilon = \left(\frac{M-M_0}{M_0}\right) \times 100 \quad (1)$$

where $\boldsymbol{\varepsilon}$ is the uptake of the electrolyte solution, M_0 is the membrane weight and M is the mass of the membrane after immersion in the electrolyte solution**.**

Impedance spectroscopy measurements were carried out into PVDF/MOFs membranes immersed of liquid electrolyte during 15 minutes at 25 ºC. The frequency ranges are between 500 mHz and 65 kHz in an AutolabPGSTAT-12 (Eco Chemie) equipment using a constant

volume support equipped with gold blocking electrodes located within a Büchi TO 50 oven. The ionic conductivity (σ_i) of the PVDF/MOFs membranes was calculated following equation:

$$\sigma_i = d/R_b \times A \quad (2)$$

where R_b is the bulk resistance, d is the thickness and A is the area of the sample.

2.6. Electrodes preparation and cycling test

Cathode preparation: The cathode was prepared using 80/10/10 wt.% of C-$LiFePO_4$, carbon black and PVDF 5130 in 2.25 mL of DMPU solvent for 1g of solid material. This electrode slurry was then casted on aluminum foil by doctor-blade technique and dried in air oven at 100 ºC for 2 h. More details about the electrode preparation are reported in [46]. The active mass loading, thickness and porosity of the electrodes were ~ 2 mg·cm^{-2}, 17 μm and 77%, respectively.

Lithium cell preparation and cycling performance: Swagelok type Li/C-$LiFePO_4$ half-cells were assembled in an argon-filled glove box where O_2 and H_2O levels were kept bellow 0.1 ppm and prepared using the PVDF/MOF-808 membranes as separator (10 mm diameter) soaked in electrolyte solution (1M $LiPF_6$ in EC:DMC, 1:1, vol). C-$LiFePO_4$ electrode was used as cathode (8 mm diameter) and metallic lithium (8 mm diameter) as anode. Galvanostatic measurements were obtained at room temperature in voltage range of 2.5 V to 4.2 V at current rates from C/5 to 2C (C = 170 mAg^{-1}) using a Landt CT2001A Instrument.

The thickness of the separator was selected to maintain its mechanical integrity as it does not affect the battery performance in the thickness range used in this work [47]. Whatman® glass microfiber separators have been selected as a commercial separator to compare their performance as they are commonly used in energy storage devices [48].

The electrical properties of the Li/C-$LiFePO_4$ half-cells before and after cycling were measured by electrochemical impedance spectroscopy (EIS) with an Autolab PGSTAT12 instrument, in frequency range from 10 mHz to 1 MHz, with an amplitude of 10 mV AC voltage signal.

To study PVDF/MOF-808 membranes stabilization with the liquid electrolyte and the Li metal electrode interface, the time dependence of the impedance response of symmetric Li / electrolyte / Li cells was evaluated under open circuit conditions.

3. RESULTS AND DISCUSSION

3.1. MOFs as active fillers

The synthesis of the MOF-808 nanoparticles was the first milestone to achieve in order to use them as active fillers for the PVDF separators. To this end, starting from the initial synthesis conditions for MOF-808 microcrystalline samples reported by Jiang *et. al.* [44], water was added to the reaction as a modulator agent (0.25 and 0.5 mL). As revealed by transmission electron micrographs (TEMs) of Figure S3a and b, water modulation of MOF-808 induces a particle reduction from micron scale crystals to 50 nm nanoparticles when 0.5 mL of water are included within the reaction media (Figure S3b).

Once obtained MOF-808 nanoparticles, the next challenge is to achieve a good colloidal stability of the MOF nanoparticles in the PVDF/N,N-Dimethylformamide solution. To this end, it was avoided drying the samples after synthesis to prevent their agglomeration, maintaining them wet after the washing and centrifugation cycles, and their posterior dispersion by ultrasound in DMF. This colloidal dispersion was used to dissolve the PVDF and to obtain the

final PVDF/MOF-808 ink. PVDF/MOF-808 separators were obtained after its solvent casting process.

3.2. Morphology, polymer phase and thermal properties of PVDF/MOFs membranes

Rietveld analyses of the PVDF and PVDF/MOF-808 patterns allows a semi-quantitative estimation of the MOF-808 nanoparticles loading within the membranes, as well as a rough determination of α and β PVDF polymorphs ratio present on the PVDF/MOF-808 composites. Figure S2 shows the final Rietveld fitting for the PVDF and PVDF/MOF-808 membranes, considering the presence of both α and β PVDF polymorphs.

Even taking into account the Rietveld analysis limitations, the results shown in the Figure S4 point that the weight percentage of MOF-808 within the membranes is slightly lower than the expected from the volume and MOF-808 concentration of the dispersions used to prepare the PVDF/MOF-808 membranes. Taking into consideration that the X-ray beam penetration within the sample is limited, the semi-quantitate results obtained from XRD data suggest a MOF-808 gradient within the membrane, being lower the MOF content at the membrane surface (Figure S4). A side effect of the MOF-808 incorporation within PVDF membranes is a slight increase of the β-phase content within the PVDF porous support; as it has been reported also for other PVDF composites based on metal oxide [49] or zeolite nanoparticles [50] for the crystallization of the γ-phase [51].

FTIR transition spectra of pure PVDF films and PVDF/MOF-808 membranes are shown in the 600-1600 cm^{-1} region in Figure 1a. Infrared spectroscopy confirms the crystallization of PVDF mainly in the α-phase. The presence of a β-PVDF phase was detected both in the initial membrane, and after including MOF-808 nanoparticles in the polymeric matrix. In addition

to the characteristic bands for the α-phase related to the rocking [52] (763 cm^{-1}) and mixed mode CF_2 bending and CCC skeletal vibration [53] (615 cm^{-1}); bands originated from mixed mode of CH_2 rocking and CF_2 asymmetric stretching vibration of β-phase, which appear at 840 cm^{-1}, are observed. No significant increase of the absorbance of 840 cm^{-1} band has been observed due to the inclusion of MOF-808 in the polymeric separators. The absence of any shoulder at 833 cm^{-1} in the same wavelength region discards the presence of the γ-PVDF phase in the composites.

Thermogravimetric analyses of the MOF-808 and PVDF/MOF-808 membranes are shown in the (Figure 1b). TGA curve of MOF-808 shows three weight loss steps associated to: i) the release of the adsorbed water molecules (30 – 100 °C), ii) the loss of the six formate groups capping six over twelve coordinative positions of the Zr hexanuclear clusters (150 -350 °C), and iii) the calcination of the trimesic organic bridges of the MOF-808 structure (450 -550 °C) Thermal decomposition of PVDF/MOF-808 membranes show a decrease of the thermal stability of the PVDF matrix due to the inclusion of MOF-808 fillers, in good agreement with previous reported results on zeolites or metal oxide nanoparticles based PVDF composites [54-55]. Indeed, the two step PVDF thermal collapse begins at 375 °C and ends at 650 °C. In composite PVDF/MOF-808 membranes, PVDF thermal decomposition is overlapped with the calcination of trimesic organic linkers of MOF-808. Nevertheless, the contribution of the MOF-808 fillers to PVDF/MOF-808 separators is clearly observed in the progressive weight loss occurring between 150 and 350°C, which is associated to the release of formic molecules.

DSC measurements are plotted in Figure 1c. The DSC curve of pure PVDF membranes only exhibits one endothermic peak corresponding to the melting of the polymer. In MOF containing membranes there is an additional endothermic peak at 60-90 °C related with the dehydration process of the MOF-808. Indeed, the integrations of the DSC peak area can be used as a tool to estimate the percentage of MOF-808 particles, which once incorporated into the PVDF matrix, are still surface active to capture water vapor from the environment. A net value of 553 $J.g^{-1}$ is obtained after the integration of the DSC peak associated to the dehydration process for MOF-808 nanoparticles (Figure S5). For the composite MOF 5, MOF 10 and MOF 15 separators exothermic processes of 18.77, 53.32 and 98.21 $J.g^{-1}$ have been obtained, close to the calculated values considering a 5, 10 and 15 % MOF loading of the membranes (Calculated MOF 5 = 27.63 $J.g^{-1}$, MOF 10 = 55.00 $J.g^{-1}$ and MOF 15 = 82.00 $J.g^{-1}$). The similarity between the estimated and experimental values confirms that near the 100 % of the MOF particles included within the separators are able to capture moisture from the environment, and hence that they are surface active to contact with the electrolyte solution once the membrane is wetted. This result points towards the possibility of considering the MOF fillers as an active part for the ion migration through the polymeric macro and meso polymeric matrix.

Figure 1c also shows that for all PVDF/MOF-808 membranes, the single peak melting behavior of the polymer occurs around at 170 °C, the MOFs not affecting the melting behavior of the PVDF polymer. The obtained 170 ºC melting temperature is between the 167 and 172 °C values reported for α and β phases, and far from the 179–180 °C melting temperature expected for the γ polymorph of PVDF.

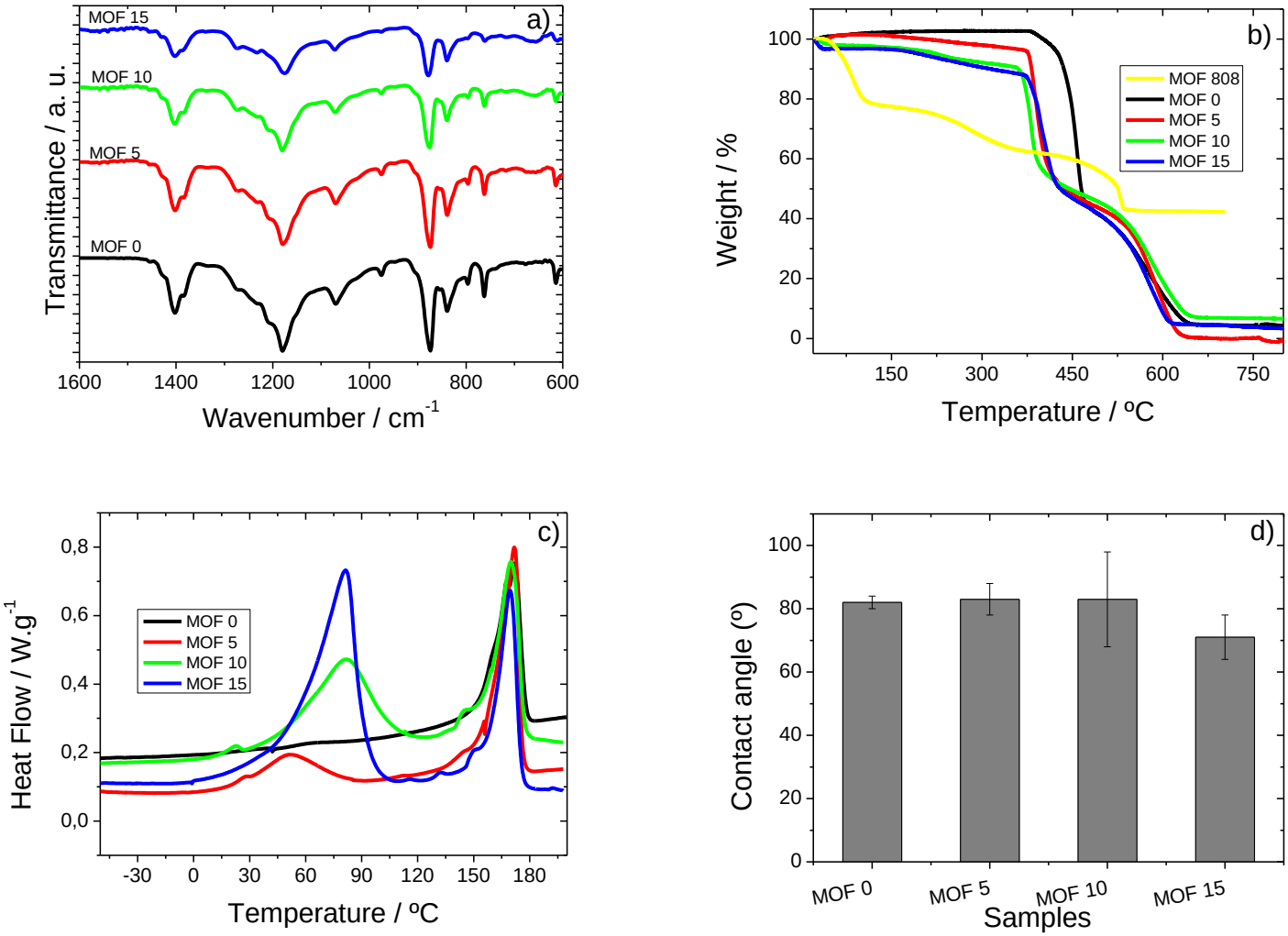

Figure 1. a) FTIR spectra, b) TGA curves, c) DSC plots and d) contact angle for neat PVDF membrane and PVDF/MOFs membranes with different MOFs contents.

The degree of crystallinity (X_c) of PVDF and the PVDF/MOF-808 nanocomposites was obtained by Equation 3:

$$X_c = \Delta H_{\mathrm{m}} \times 100 \times (\Delta H_{100\%\,\mathrm{cystalline}})_{\alpha} + (\Delta H_{100\%\,\mathrm{cystalline}})_{\beta} \qquad (3)$$

where x and y corresponds to the weight fraction of the α- and β-phase, respectively, and $(\Delta H_{100\%\,\text{cystalline}})_{\alpha}$ and $(\Delta H_{100\%\,\text{cystalline}})_{\beta}$ are the melting enthalpies for 100% crystalline α- and β-PVDF= 93.04 and 103.4 $J \cdot g^{-1}$, respectively [51].

Further, the calculated degree of crystallinity of the polymer is between 40 % to 50 %, being lower for the higher MOFs contents, which indicate that the MOFs induce defects in the polymer arrangement during its crystallization process [56]. MOF-808 nanoparticles can endow PVDF membrane of some degree of hydrophilicity, which can be detected by water contact angle measurements (Figure 1d and Figure S6). It is shown that the roughness of the surface in the MOF – PVDF composites (Figure S6) increase the uncertainty of the obtained contact angle values; but a significant reduction is observed for the sample with the highest MOF loading.

The porous structure of the PVDF/MOF-808 membranes was studied by means of SEM surface and cross-section images. MOF 0, 5, 10 and 15 membranes (Figure 2) show the porous nature of the PVDF separator, independently of the MOF loading, but the surface and cross section structure is affected by the nanoparticle's inclusion.

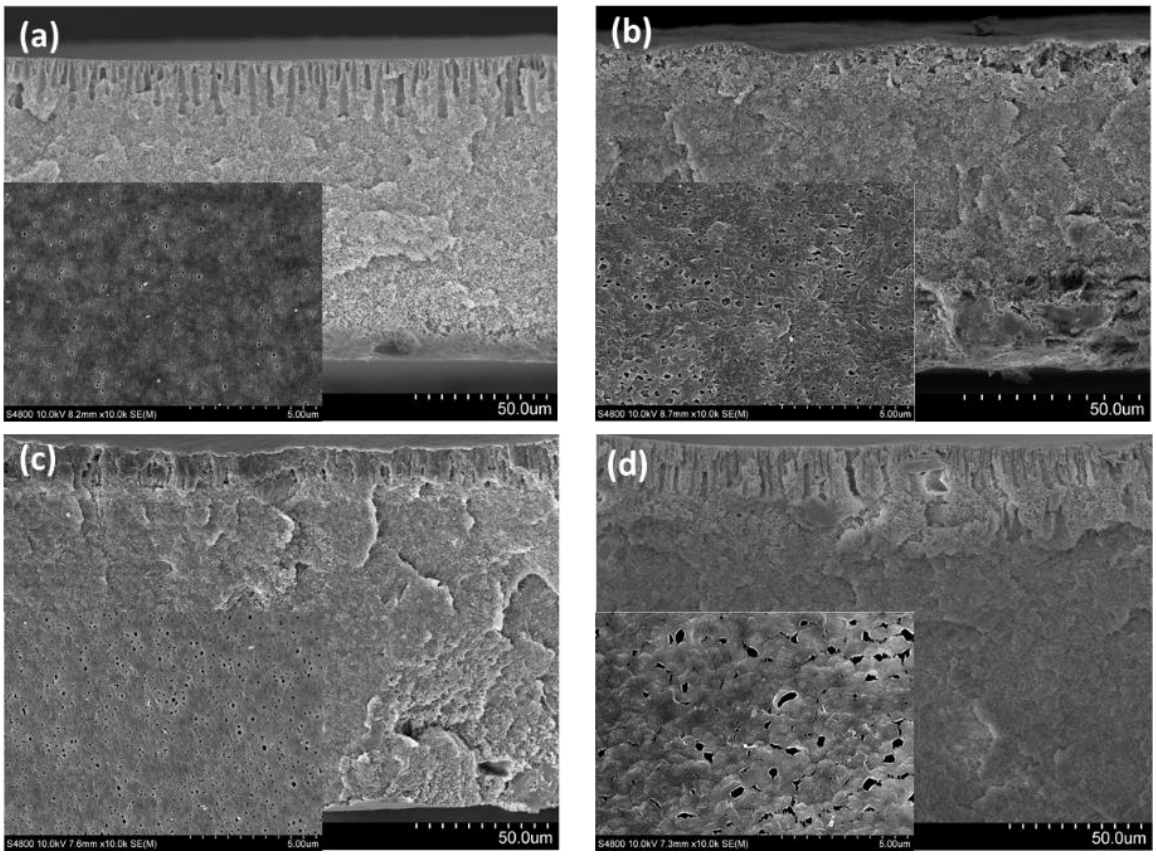

Figure 2. Cross-section and surface (inset images) scanning electron microscopy images of MOF 0 (a), 5 (b), 10 (c) and 15 (d) membranes.

A more irregular porous channeled section near the surface is observed for MOF-808 loaded membranes; a trend that is confirmed by the surface SEM images (Inset Figure 2); where a size increase and a more random and heterogeneous distribution of the pores is observed. This trend is highly accentuated for the MOF 10 to 15 membrane.

Regarding the mechanical properties, the separators can be manually twisted, folded and stretched without deformation or cracking and have adequate mechanical stability (>1 MPa) to be used as separator in LIBs [57].

3.3. Porosity, electrolyte uptake, ionic conductivity and electrochemical window

Figure 3a and 3b shows the intruded and intruded cumulative volume dependence of the pore size in PVDF/MOF-808 membranes. All the samples exhibit a bimodal pore distribution centered at 0.3 and 100 μm. Approximately, the 20% of the porous volume is associated to pore diameters between 20-200 μm whilst the other 80% is related to the smaller macropores regime between 1 and 0.01 μm. The MOF-808 nanoparticles induce a displacement of both peaks of the pore diameters bimodal distribution to lower values, that is, the pore size in both regimes becomes smaller. A small increase of the volume of mercury intruded at the mesopore scale (20 Å) is observed as the MOF-808 content in the PVDF separators increase. In the same line that the information obtained from SEM images, the increase of the MOF-808 content up to 15% leads to a more inhomogeneous porosity of the PVDF separator. Indeed, macro-pores with intermediate diameters are generated in the membranes, and the pore size distribution of the large macro-pore regime becomes more irregular. Therefore, the modulator role of the MOF-808 nanoparticles is well proven, since in addition to increase the total porous volume of the system, they lead also to a reduction of the macro-pores´ size. On the contrary, the higher the content of the MOF-808, the higher the heterogeneity of the macropore structure of the PVDF, being this effect particulary enhanced between the MOF 10 and 15 separators. The trend drawn by mercury porosimetry measurements is in line with the PVDF structure changes previously described with respect to the scanning electron microscopy images.

Considering that MOF-808 solely exhibits surface areas near 2000 m^2/g; apart from the surface area gain related to the MOF/polymer structure, a neat increase of 100 (MOF 5), 200 (MOF 10), and 300 m^2/g (MOF 15) in the total surface area ascribed to the MOF nanoparticles is foreseen (Figure 3c). We have tried to corroborate these values experimentally by N_2

(77K) and CO_2 (293 K) sorption measurements without success. The MOF-808 material activation process has been limited to 100ºC during 24h, in order to minimize as much as possible, the porous structure modification of the PVDF polymeric matrix during the process. Nevertheless, it seems that the activation process alters somewhat the membrane structure blocking the access of the N_2/CO_2 to the MOF-808 nanoparticles, since isotherms show a negligible adsorption in the micro-porous regime because the ineffective activation protocol.

The increase in surface area and total porosity of the PVDF/MOF-808 is not directly reflected in the electrolyte uptake percentage, as observed in Figure 3d. An initial increase of electrolyte uptake from 300 % for MOF 0 to 400 for MOF 5 %, a further MOF loading in MOF 10 and MOF 15 membranes induce an electrolyte uptake reduction to 200 and 250 %. Therefore, the electrolyte wettability degree of PVDF/MOF separator not only depends on the total porosity, but on the effective total porous structure that can be accesses by the electrolyte. Assuming that the porosity of the MOF 0 (0.22 cc/g) in completely accessible, it can be estimated that MOF 5, 10 and 15 exhibit a 92% (0.29 cc/g), 38% (0.15 cc/g) and 37 % (0.185 cc/g) of their pore volume accessible by the electrolyte. Thus, the electrolyte uptake is governed not by the total porosity but for the porous structure homogeneity and inter-connection.

Nevertheless, for all cases, the porosity percentage and electrolyte uptake capacity are much higher than the usual porosity of commercial battery separators based on PP, PP/PE porous membranes (i.e. 40 – 85 % total porosity [8, 10, 14]); and it is even superior for MOF 5 and MOF 10 than the electrolyte uptake capacity reported for PVDF/MOF-74 separator (256 %) used in Li-S batteries by D. Han et. al. [41].

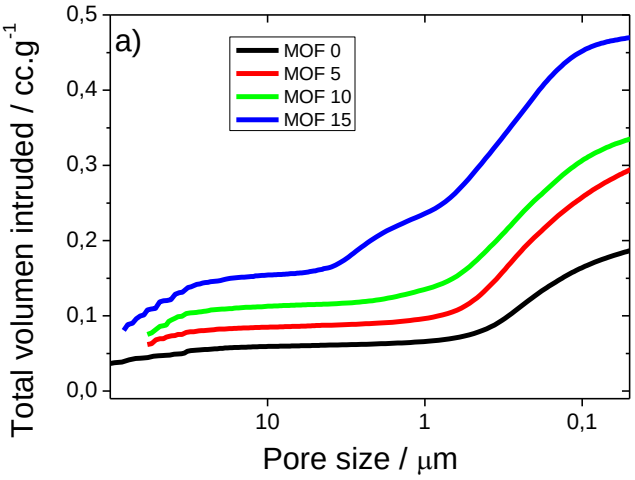
a)
MOF 0
MOF 5
MOF 10
MOF 15
Total volumen intruded / cc.g-1
Pore size / μm

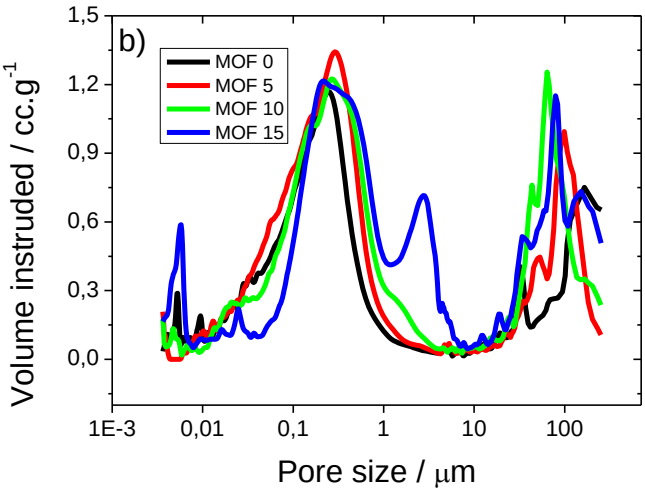
b)
MOF 0
MOF 5
MOF 10
MOF 15
Volume instruded / cc.g-1
Pore size / μm

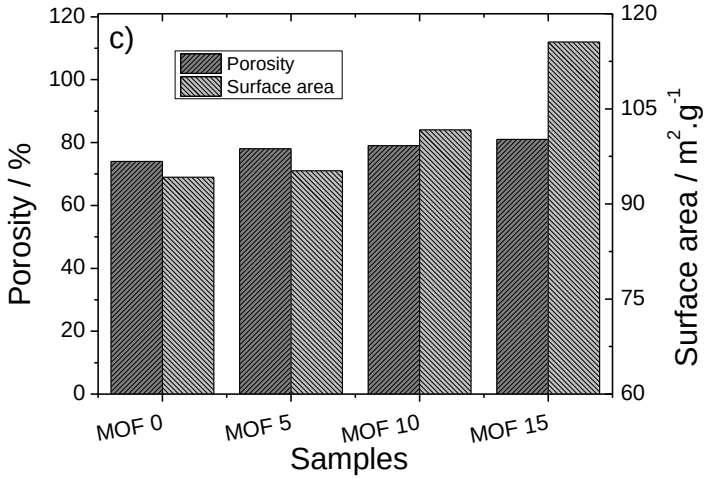
c)
Porosity
Surface area
Porosity / %
Surface area / m2.g-1
MOF 0
MOF 5
MOF 10
MOF 15
Samples

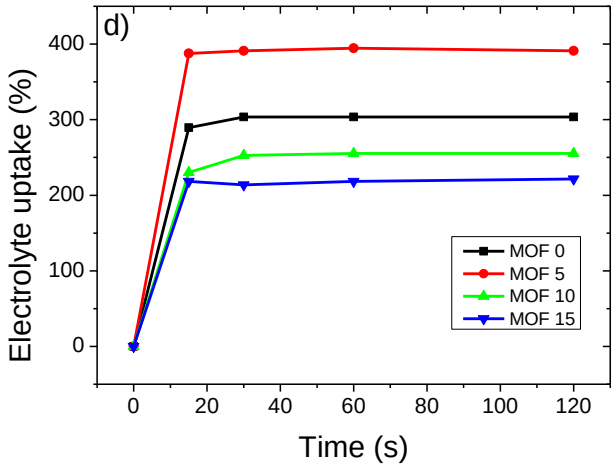
d)
MOF 0
MOF 5
MOF 10
MOF 15
Electrolyte uptake (%)
Time (s)

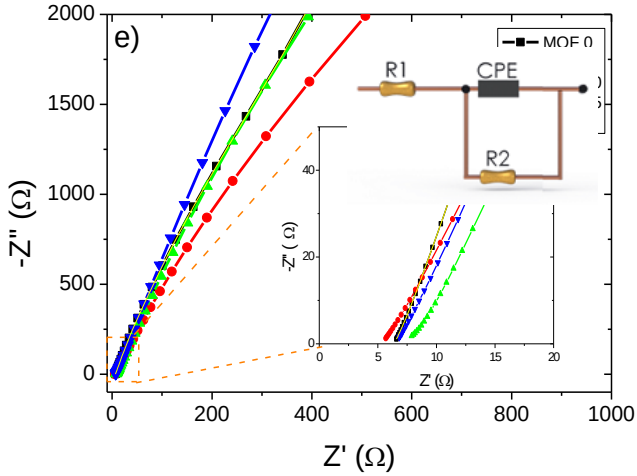
e)
R1
CPE
R2
-Z'' (Ω)
Z' (Ω)

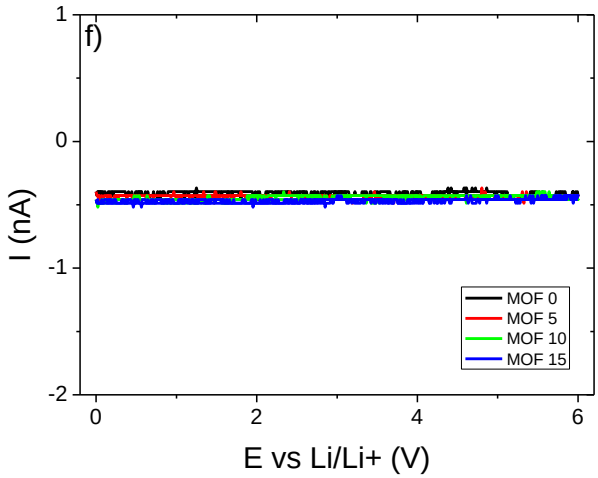
f)
MOF 0
MOF 5
MOF 10
MOF 15
I (nA)
E vs Li/Li+ (V)

Figure 3. a) Intruded and b) Intruded cumulative volume dependence of the pore size, c) porosity, d) electrolyte uptake percentage as function of time, e) Nyquist plot and f) cyclic voltammogram in the 0.0 to 6.0 V Li/Li^+, for all the prepared samples.

The ionic conductivity of neat PVDF and PVDF/MOFs membranes was determined by impedance spectroscopy at 25 ºC, reported in Figure 3e as Nyquist plots for the different membranes. Independently on the membrane, the AC response exhibits an inclined straight-line (typical of the blocking electrode capacitive behavior) whose intercept with the real axes, Z', gives the PVDF-based electrolyte membrane ionic resistance [58]. This value was obtained through analysis of the impedance responses, performed using a common approach, i.e., by defining an equivalent circuit taking into account all possible contributions to the impedance of the membranes, which is constituted by two elements connected in series, e.g., the electrolyte bulk resistance (R) and the double layer capacitance at the electrolyte/electrode interface (Qdl). A constant-phase element, CPE (Q), was used in the place of pure capacitance (C) [58].

The ionic conductivity values, reported in Table 1 and calculated by equation 2, are above 10^{-3} S cm^{-1}, indicating suitable transport properties within the PVDF/MOFs membranes for battery applications [59]. The addition of MOFs to the PVDF membrane affects the ion conduction depending on the ability to trap liquid electrolyte, which is the largest for MOF 5 (Figure 3d), resulting in higher electrical conductivity through the PVDF/MOFs membrane with respect to the neat porous membrane sample [60]. This linear trend, plotted in the Figure S7, is also followed by the MOF 15 sample, which show lower conductivity values than the net PVDF membrane. Surprisingly, the MOF 10 sample shows much higher conductivity

values than expected based on its electrolyte uptake capacity. Taking into consideration that both MOF 0, 5 and 10 samples show a homogeneous porous structures with well-defined bimodal distributions, this fact points to the beneficial effect of the MOF-808 nanoparticle fillers, despite further studies are needed to understand in deep their specific role in the lithium transport.

Table 1. Ionic conductivity value for the different PVDF/MOFs membranes.

Sample	σi / $mS.cm^{-1}$
MOF 0	3.5
MOF 5	4.2
MOF 10	3.8
MOF 15	2.9

To evaluate the electrochemical stability window, cyclic voltammetry (CV) was performed in asymmetric cells with linear cyclic voltammogram in the 0.0 to 6.0 V Li/Li^+ for all the prepared samples confirm the excellent electrochemical stability of PVDF/MOF separators under cycling without electrochemical oxidation at anodic potentials lower than about 6V (Figure 3f).

3.4. Cycling behavior

$Li/LiFePO_4$ half-cells with the PVDF/MOFs membranes were cycled at various C rates (C/5 at 2C) between 2.5 and 4.2 V and the charge-discharge voltage profiles for MOF 10 sample are shown in Figure 4a displaying just the fifth curve for each rate, for the demonstration of their suitability as separator for lithium-ion batteries applications. Just the charge-discharge

profiles for the 10 % MOF-808 membrane is presented as for the other samples the behavior are similar. Initial results show that at low C-rates the performance of the PVDF/MOF-808 composite separator is similar independently on their conductivity values or electrolyte uptake. The scenario changes at high rates, since the combination of all the characteristics of the membranes influence their performance, not only the ionic conductivity itself. In this case, the MOF 10 samples has revealed as the most stable separator, showing MOF 5 an intermediate behavior between MOF 10 and MOF 0 separators (Figure 4b). The electrochemical performance of the MOF/PVDF separators is improved until a threshold where the MOF nano-fillers introduce too much heterogeneities in the macro-porous structure of the separator, For that, the cycling performance of the MOF 10 based cell was studied up to 100 cycles (Figure 4c).

A typical flat voltage plateau around 2-3 to 3.6 V in the charge-discharge behavior is observed in Figure 4a in the presence of a Fe_2^+/Fe_3^+ redox reaction between $FePO_4$ and $LiFePO_4$ [61]. This behavior is independent of the scan rate and cycle number. It is also observed that the charge/discharge profiles decrease with increasing scan rate due to the influence of ion transport on Ohmic polarization and the reaction resistance of the interface between electrode and electrolyte (Figure 4b) [62].

Figure 4b shows the rate capacities of the Li/C-$LiFePO_4$ cells using neat membrane (MOF 0) and PVDF/MOFs separators (MOF 5, MOF 10, MOF 15) at C/8, C/5, C/2, C, and 2C rates for 10 cycles. Discharge capacity is similar for all separators at low C/8 and C/5 rates; with values near 140 $mAh.g^{-1}$. At higher rates above C/2-rate, the discharge capacity gradually decreases due to lithium migration limitations, but the capacity fading is much less pro-

nounced for MOF 5, and especially for MOF 10 composite separators due to ionic conductivity value and uptake process. In principle, the MOF 5 membranes should work better taking into account its ionic conductivity and electrolyte uptake values. The battery performance of PVDF-MOF 808 separators has been compared with commercial glass microfiber separators, which are used in various lithium-ion battery systems, as shown in Figure 4b. It is observed that at C-rates above C the discharge value of the PVDF-MOF 808 separators is higher than the one for the glass microfibre separator.

Nevertheless, it seems that the more regular and homogeneous structure of the MOF 10 sample, with ionic conduction and electrolyte uptake capacity close to the one of neat PVDF, play an important role in the lithium migration mechanisms at high C/rates. It is observed that 10 wt% of MOFs is found to be an adequate amount to obtain higher discharge capacity values when compared to other membranes. The improved rate performance of PVDF/MOFs membranes with 10wt% is ascribed to the combination of the proper macro and mesoporous structure, efficient ionic mobility of lithium ions (that accounts for a part of the determined ionic conductivity), and the rapid transport of Li ions at the interface between the electrodes and electrolyte. The hydrophilic character of MOF-808 fillers favors the wettability of the membranes at the macroscopic scale; and it is foreseen that the presence of acid positions at the inner space and surface of the MOF-808 serve as lithium docking and jumping points favoring the lithium migration through the separator. Nevertheless, further research is needed to confirm this. Also, independently on the separator type, initial discharge capacity values are recovered when cycling at low C/8 rates (Figure 4b).

Taking into account the highest discharge value for the PVDF/MOFs membrane with 10 wt% of MOFs as a 100 % capacity value, Figure 4c shows the cycling performance at C rate for

this sample over 100 cycles. Figure 4c shows a significant capacity loss above the 10th cycle, but after the 20th cycle the discharge capacity is stabilized near a 55 $mAh.g^{-1}$, with a small loss down to 50 $mAh.g^{-1}$ values up to the 100 cycle. Coloumbic efficiency is highly stable during all the cycling study with values near the 98%.

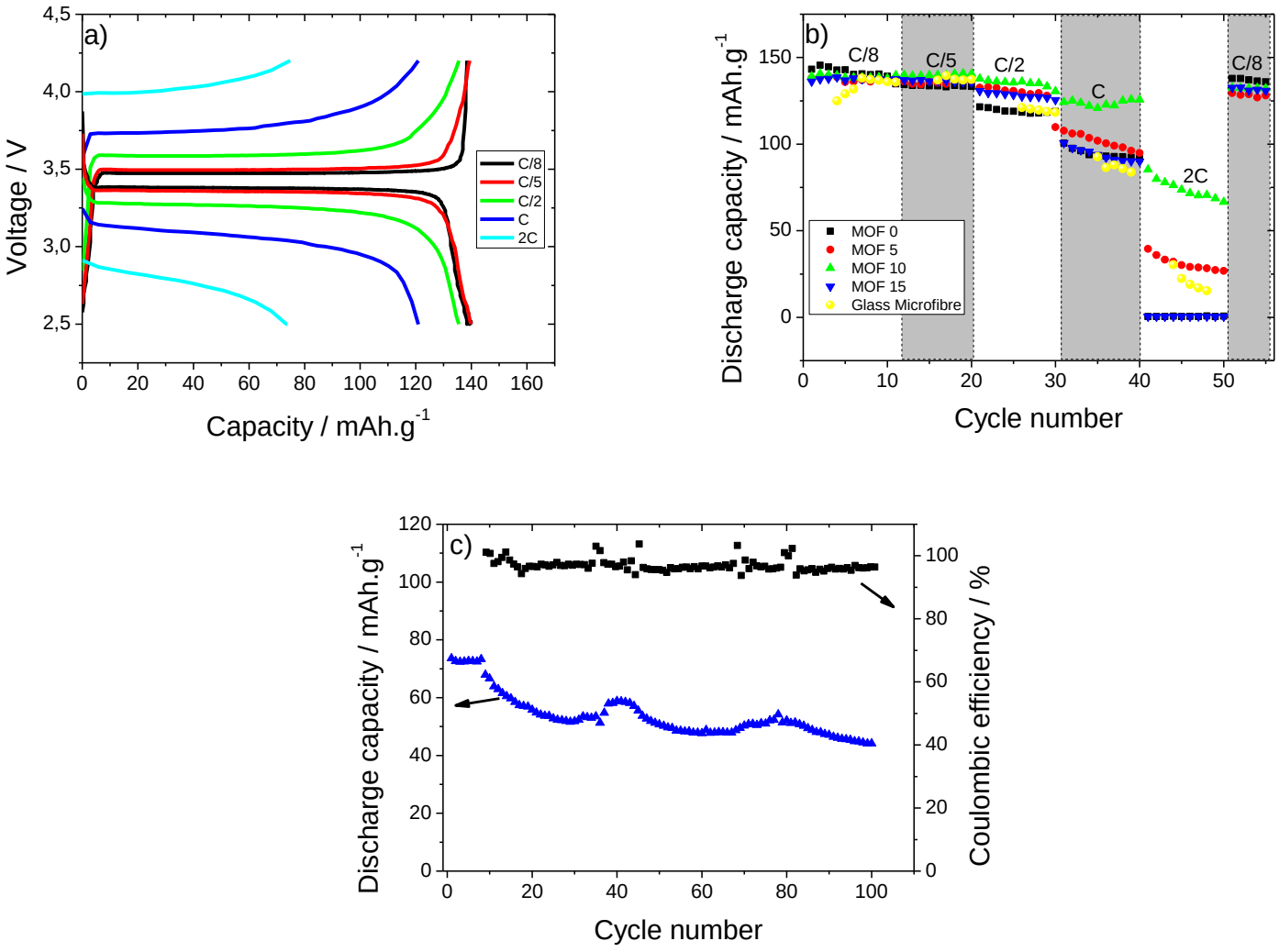

Figure 4. a) Galvanostatic charge/discharge curves for the MOF 10 sample, b) rate capacity between C/8- and 2C- rate and c) cycling performance at C-rate and its coulombic efficiency for the MOF 10 sample.

From a global perspective, the PVDF/MOF separators presents an excellent performance in $LiFePO_4$ half-cells and comparable to commercial separators. More probably, providing the PVDF membrane with an anisotropic structure could protect the membrane from lithium puncturing in the long-term, but in return could also difficult the migration of the electrolyte components through the dense PVDF skin of the membrane. Nevertheless, the potential in terms of chemical tuneability of the membranes, and hence on the enhancement of the ion mobility within the PVDF/MOF system, are quite large due to the chemical versatility of the MOF chemistry. It is worthy to mention that a significant improvement in comparison to the neat PVDF membranes has been achieved just by varying the MOF-808 nanoparticles content to 10 %wt. Therefore, it is foreseen that implementing the PVDF/MOF porous structure (TIPS; NIPS, electrospinning…), and afterwards, tailoring the MOF material of the proper surface and inner chemistry, the PVDF/MOF technology could even further improve the performance reported in this study.

Considering the cycling behavior presented in Figure 4 for PVDF/MOFs composites, Table S1 compares the electrochemical properties of the porous membranes with MOFs fillers for battery systems reported in the literature.

The MOFs as filler templates for battery separators have been used for several lithium battery systems, from the more recently explored Li-S [63] and Li-air batteries [64], to the classic systems based on $LiFePO_4$ as cathode electrode [33, 65]. In general terms, the electrochemical behavior, cycling stability, and performance at high rates of MOF-separator composites overcome the performance of pure polymeric membranes (Figure 5 and Table S1); but it is important to take into account that the role of the MOF fillers in each system is completely different. For

Li-S batteries, MOF act as a molecular sieve incorporated within the separator, blocking the pass of polysulfide through the separator to the lithium metallic anode [43, 66]. For lithium air batteries, the MOF fillers at the separators act also as a sieve to favors the pass of O_2 and prevent the permeation of atmospheric CO_2 and H_2O molecules to the Li-air systems; since CO_2 and H_2O are well known poisons for metallic lithium anode [67]. The function of MOFs in battery separators of classic lithium- $LiFePO_4$ cells differs from the molecular sieve one described previously. In solid PEO electrolytes [68], MOFs mainly acts as an enhancers of the lithium conductivity and migration through the system; whilst in porous separators wetted in classic liquid electrolytes [33]; the MOFs act also as a modifiers of the surface chemistry of the separators improving the wettability and lithium transport during operation.

In order to better understand the cycling behavior of $Li/LiFePO_4$ half-cells with PVDF/MOFs membranes, the electrochemical impedance spectroscopy spectra of these half-cells were recorded before and after cycling and are shown in Figure 5a-b, respectively.

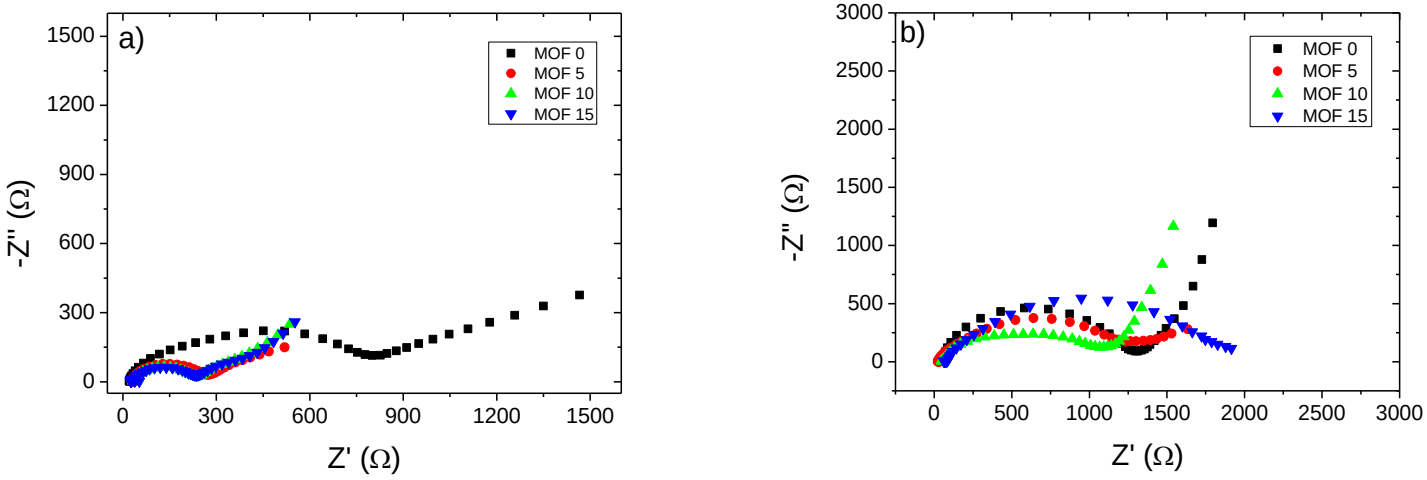

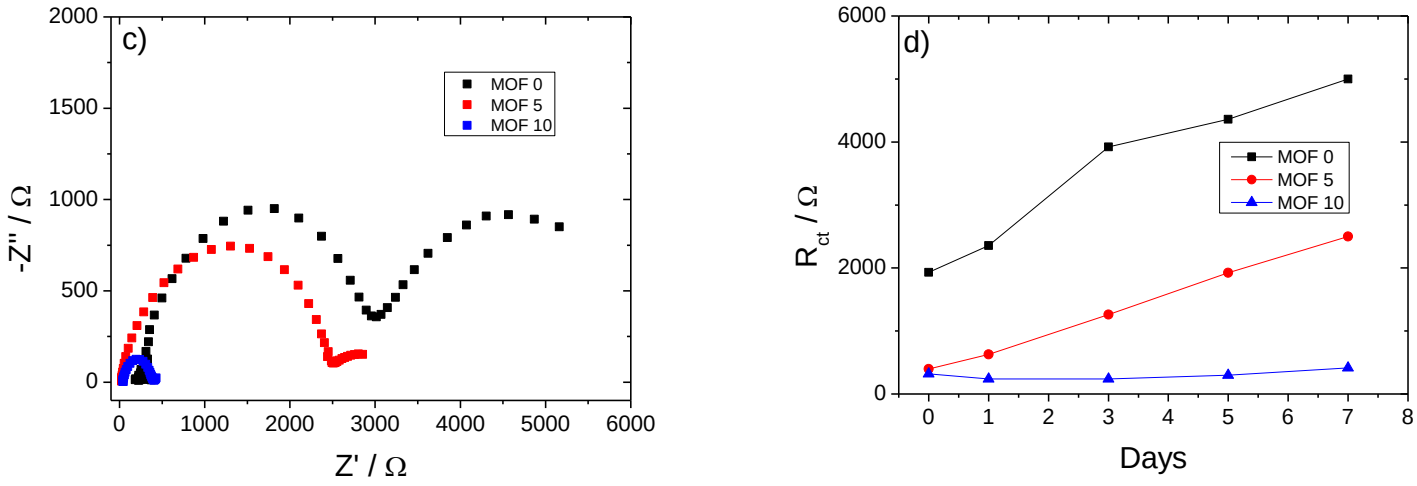

Figure 5. a) EIS curve before and b) after cycling, for the different samples. c) Li/Li formation after 7 days and d) evolution of the resistance over time up to 7 days.

Figure 5a-b show the Nyquist plot that is characterized by a semicircle that represents the overall resistance. This overall resistance represents the sum of the Ohmic resistance, the contact film resistance, and resistance contributions from the charge-transfer reactions in the high and medium frequency regions. Further, it is also characterized by a straight line that is associated of the Li^+ diffusion process in the low frequency regions [69]. This behavior is also observed for all PVDF/MOFs separators.

Before cycling (Figure 5a), it is observed that the PVDF/MOF-808 composite membranes has a lower resistance value (240 Ω) in comparison to the net PVDF separator. After cycling (Figure 5b), it is observed an increase in the overall resistance for all membranes due to the formation of solid electrolyte interface (SEI) layer [69]. It is worth to noticing that before and after cycling the PVDF/MOF-808 membrane with the lower resistance value is the one

loaded with a 10 wt% of MOF fillers is due to the small growth of the SEI layer between electrode and separator.

Li/Li symmetric cell with PVDF/MOFs separator at 25 ºC was used to study the chemical stability by monitoring the impedance over time, as shown Figure 5c and d. The Nyquist plot after 7 days for the separator with 15% wt of MOF is identical to that observed for the neat PVDF membrane. Figure 5c shows the Nyquist plot after 7 days. The behavior of the PVDF/MOFs membrane with 15 wt% is similar to that observed for 5wt% MOF membrane. Typically, the EIS spectrum consists of two flat semicircles that reflect electrochemical reactions that occurs at the separator–lithium interface [70]. It is observed that the addition of MOFs in the PVDF polymer matrix reduces the interfacial resistance compared to the neat membrane, the MOFs improving the ionic conduction in the passivation layer and the lithium charge-transfer processes at the separator–lithium interface (Figure 5d). Further work is ongoing to confirm by impedance spectroscopy if the PVDF/MOFs membrane with 10 wt% acts as an active separator able to block lithium dendrites growth (Figure 5d).

Summarizing, the interplay of different factors determines the final performance of the PVDF/MOF systems, in particular when exploring the performance of the cells at high rates, and in the long-term cycling. Thus, the approach applied in this work is promising since it confirms the templating effect of MOF-808 fillers loading on the porous structure and surface chemistry of the separator composite systems; but also the impact of incorporating a zirconium-based MOF with high degree of open positions within its crystal structure, which has been shown to be beneficial in terms of lithium effective transport and battery cycling stability. Moreover, once stablished the proof of concept, PVDF/MOF-808 composites can serve

as easily post-synthetically modifiable platforms; since different anionic groups can be anchored post-synthetically; even after immobilizing the MOF-808 nanoparticles at the PVDF supports.

4. CONCLUSIONS

This work shows that MOF-808 nanoparticles can be used as active fillers to modify the macro and meso porosity of PVDF separators. The inclusion of MOF-808 nanoparticles slightly influence the asymmetric macro and mesoporous structure of the PVDF membranes, increasing their total porosity and surface area. MOF-808 has been also revealed as active components of the separators that are fully in contact with the surface of the porous membrane. Once embedded, MOF-808 nanoparticles influence the pore chemistry of PVDF supports adding wettability and electrolyte capacity storage to the system. Jointly, the structural, surface and conductive characteristics of the composite separators facilitate lithium migration paths through the whole composite system enhancing the long-term high rate cycling stability of the cell.

The presence of the MOF-808 at the PVDF separators reduces the resistivity of the separators and separator-electrolyte systems. Independently on the MOF-808 loading, the membranes maintain a broad electrochemical stability window. The evaluation of the discharge capacity of the cells points that the PVDF/MOF-808 separators makes the difference at high rates cycling, preventing the full capacity fading of the cell, as occurred for PVDF separator. In addition, the MOF 10 separator shows a good cycling stability above the 20th cycle, while maintaining a coulombic efficiency near 100 %. After cycling, the resistivity values of PVDF/MOF-808 based cells still are lower than these for pure polymeric systems.

The proof of concept study presented in this work is promising, since starting from the developed PVDF/MOF-808 systems, and taking into consideration the chemistry plasticity offered by MOFs, a plenty of opportunities arises to modify the structure and chemistry of polymeric separators to tune the specific electrolyte – polymeric support interaction.

ASSOCIATED CONTENT

Supporting Information. "This material is available free of charge via the Internet at http://." Description: Additional characterization measurements for the MOF-808 and PVDF membranes. Comparative table of other MOF-polymer separator systems.

AUTHOR INFORMATION

Corresponding Author

cmscosta@fisica.uminho.pt (Carlos M. Costa)

roberto.fernandez@bcmaterials.net (Roberto Fernández de Luis)

Author Contributions

The manuscript was written through contributions of all authors. All authors have given approval to the final version of the manuscript.

ACKNOWLEDGMENT

The authors thank the FCT (Fundação para a Ciência e Tecnologia) for financial support under the framework of Strategic Funding grants UID/FIS/04650/2019, and UID/QUI/0686/2019 and project PTDC/FIS-MAC/28157/2017. The author also thanks the FCT for financial support under grant SFRH/BPD/112547/2015 (C.M.C.) and Investigator FCT Contract CEECIND/00833/2017 (R.G.). A.V. thanks to the Basque Government Education department for her pre-doctoral grant. The European Commission Research & Innovation H2020-MSCA-RISE-2017 (Ref.: 778412) INDESMOF project is also acknowledged. Financial support from the Basque Government Industry and Education Departments under the ELKARTEK (ACTIMAT and LION), HAZITEK (SIMAM) and PIBA (PIBA-2018-06-LIMOFILM) programs, respectively, is also acknowledged.

REFERENCES

1. Besenhard, J. O. *Handbook of Battery Materials*. Wiley: **2008**.
2. Eurostat *Renewable energystatistics*; **2020**.
3. Lv, F.; Wang, Z.; Shi, L.; Zhu, J.; Edström, K.; Mindemark, J.; Yuan, S. Challenges and development of composite solid-state electrolytes for high-performance lithium ion batteries. *Journal of Power Sources* **2019,** *441*, 227175.
4. Costa, C. M.; Lee, Y.-H.; Kim, J.-H.; Lee, S.-Y.; Lanceros-Méndez, S. Recent advances on separator membranes for lithium-ion battery applications: From porous membranes to solid electrolytes. *Energy Storage Materials* **2019,** *22*, 346-375.
5. Nunes-Pereira, J.; Costa, C. M.; Lanceros-Méndez, S. Polymer composites and blends for battery separators: State of the art, challenges and future trends. *Journal of Power Sources* **2015,** *281*, 378-398.
6. Lagadec, M. F.; Zahn, R.; Wood, V. Characterization and performance evaluation of lithium-ion battery separators. *Nature Energy* **2019,** *4*, 16-25.

7. Lagadec, M. F.; Zahn, R.; Müller, S.; Wood, V. Topological and network analysis of lithium ion battery components: the importance of pore space connectivity for cell operation. *Energy & Environmental Science* **2018,** *11*, 3194-3200.

8. Abraham, K. M.; Alamgir, M.; Hoffman, D. K. Polymer Electrolytes Reinforced by Celgard® Membranes. *Journal of The Electrochemical Society* **1995,** *142*, 683-687.

9. Martinez-Cisneros, C.; Antonelli, C.; Levenfeld, B.; Varez, A.; Sanchez, J. Y. Evaluation of polyolefin-based macroporous separators for high temperature Li-ion batteries. *Electrochimica Acta* **2016,** *216*, 68-78.

10. Hantel, M. M.; Armstrong, M. J.; DaRosa, F.; l'Abee, R. Characterization of Tortuosity in Polyetherimide Membranes Based on Gurley and Electrochemical Impedance Spectroscopy. *Journal of The Electrochemical Society* **2017,** *164*, A334-A339.

11. l'Abee, R.; DaRosa, F.; Armstrong, M. J.; Hantel, M. M.; Mourzagh, D. High temperature stable Li-ion battery separators based on polyetherimides with improved electrolyte compatibility. *Journal of Power Sources* **2017,** *345*, 202-211.

12. Valøen, L. O.; Reimers, J. N. Transport Properties of LiPF6-Based Li-Ion Battery Electrolytes. *Journal of The Electrochemical Society* **2005,** *152*, A882-A891.

13. Zugmann, S.; Fleischmann, M.; Amereller, M.; Gschwind, R. M.; Wiemhöfer, H. D.; Gores, H. J. Measurement of transference numbers for lithium ion electrolytes via four different methods, a comparative study. *Electrochimica Acta* **2011,** *56*, 3926-3933.

14. Zahn, R.; Lagadec, M. F.; Hess, M.; Wood, V. Improving Ionic Conductivity and Lithium-Ion Transference Number in Lithium-Ion Battery Separators. *ACS Applied Materials & Interfaces* **2016,** *8*, 32637-32642.

15. Zhu, W.; Wang, Z.; Qiu, W.; Xiang, Y.; Du, Y.; Liu, D.; Qu, D.; Xie, Z.; Tang, H.; Li, J. Improving the Electrochemical Performance of Polypropylene Separator through Instantaneous Photo-Induced Functionalization. *Journal of The Electrochemical Society* **2018,** *165*, A1909-A1914.

16. Wu, D.; Deng, L.; Sun, Y.; Teh, K. S.; Shi, C.; Tan, Q.; Zhao, J.; Sun, D.; Lin, L. A high-safety PVDF/Al2O3 composite separator for Li-ion batteries via tip-induced electrospinning and dip-coating. *RSC Advances* **2017,** *7*, 24410-24416.

17. Zhang, F.; Ma, X.; Cao, C.; Li, J.; Zhu, Y. Poly(vinylidene fluoride)/SiO2 composite membranes prepared by electrospinning and their excellent properties for nonwoven separators for lithium-ion batteries. *Journal of Power Sources* **2014,** *251*, 423-431.

18. Li, H.; Li, L.; Zheng, S.; Wang, X.; Ma, Z. High Temperature Resistant Separator of PVDF-HFP/DBP/C-TiO2 for Lithium-Ion Batteries. *Materials* **2019,** *12*, 2813.

19. Yeon, D.; Lee, Y.; Ryou, M.-H.; Lee, Y. M. New flame-retardant composite separators based on metal hydroxides for lithium-ion batteries. *Electrochimica Acta* **2015,** *157*, 282-289.

20. Liu, W.; Lin, D.; Sun, J.; Zhou, G.; Cui, Y. Improved Lithium Ionic Conductivity in Composite Polymer Electrolytes with Oxide-Ion Conducting Nanowires. *ACS Nano* **2016,** *10*, 11407-11413.

21. Kim, Y.; Kwon, S. J.; Jang, H.-k.; Jung, B. M.; Lee, S. B.; Choi, U. H. High Ion Conducting Nanohybrid Solid Polymer Electrolytes via Single-Ion Conducting Mesoporous Organosilica in Poly(ethylene oxide). *Chemistry of Materials* **2017,** *29*, 4401-4410.

22. Li, W.; Zhang, S.; Wang, B.; Gu, S.; Xu, D.; Wang, J.; Chen, C.; Wen, Z. Nanoporous Adsorption Effect on Alteration of the Li+ Diffusion Pathway by a Highly Ordered Porous Electrolyte Additive for High-Rate All-Solid-State Lithium Metal Batteries. *ACS Applied Materials & Interfaces* **2018,** *10*, 23874-23882.

23. Xiao, W.; Gong, Y.; Wang, H.; Zhao, L.; Liu, J.; Yan, C. Preparation and electrochemical performance of ZrO2 nanoparticle-embedded nonwoven composite separator for lithium-ion batteries. *Ceramics International* **2015,** *41*, 14223-14229.

24. Freund, R.; Lächelt, U.; Gruber, T.; Rühle, B.; Wuttke, S. Multifunctional Efficiency: Extending the Concept of Atom Economy to Functional Nanomaterials. *ACS Nano* **2018,** *12*, 2094-2105.

25. Furukawa, H.; Cordova, K. E.; O'Keeffe, M.; Yaghi, O. M. The Chemistry and Applications of Metal-Organic Frameworks. *Science* **2013,** *341*, 1230444.

26. Maurin, G.; Serre, C.; Cooper, A.; Férey, G. The new age of MOFs and of their porous-related solids. *Chemical Society Reviews* **2017,** *46*, 3104-3107.

27. Ribeiro, C.; Costa, C. M.; Correia, D. M.; Nunes-Pereira, J.; Oliveira, J.; Martins, P.; Gonçalves, R.; Cardoso, V. F.; Lanceros-Méndez, S. Electroactive poly(vinylidene fluoride)-based structures for advanced applications. *Nature Protocols* **2018,** *13*, 681-704.

28. Bai, Y.; Dou, Y.; Xie, L.-H.; Rutledge, W.; Li, J.-R.; Zhou, H.-C. Zr-based metal–organic frameworks: design, synthesis, structure, and applications. *Chemical Society Reviews* **2016,** *45*, 2327-2367.

29. Morris, W.; Volosskiy, B.; Demir, S.; Gándara, F.; McGrier, P. L.; Furukawa, H.; Cascio, D.; Stoddart, J. F.; Yaghi, O. M. Synthesis, Structure, and Metalation of Two New Highly Porous Zirconium Metal–Organic Frameworks. *Inorganic Chemistry* **2012,** *51*, 6443-6445.

30. Wang, S.; Wahiduzzaman, M.; Davis, L.; Tissot, A.; Shepard, W.; Marrot, J.; Martineau-Corcos, C.; Hamdane, D.; Maurin, G.; Devautour-Vinot, S.; Serre, C. A robust zirconium amino acid metal-organic framework for proton conduction. *Nature Communications* **2018,** *9*, 4937.

31. Valenzano, L.; Civalleri, B.; Chavan, S.; Bordiga, S.; Nilsen, M. H.; Jakobsen, S.; Lillerud, K. P.; Lamberti, C. Disclosing the Complex Structure of UiO-66 Metal Organic Framework: A Synergic Combination of Experiment and Theory. *Chemistry of Materials* **2011,** *23*, 1700-1718.

32. Chavan, S.; Vitillo, J. G.; Uddin, M. J.; Bonino, F.; Lamberti, C.; Groppo, E.; Lillerud, K.-P.; Bordiga, S. Functionalization of UiO-66 Metal−Organic Framework and Highly Cross-Linked Polystyrene with Cr(CO)3: In Situ Formation, Stability, and Photoreactivity. *Chemistry of Materials* **2010,** *22*, 4602-4611.

33. Shen, L.; Wu, H. B.; Liu, F.; Zhang, C.; Ma, S.; Le, Z.; Lu, Y. Anchoring anions with metal–organic framework-functionalized separators for advanced lithium batteries. *Nanoscale Horizons* **2019,** *4*, 705-711.

34. Pang, Q.; Tu, B.; Li, Q. Metal–organic frameworks with multicomponents in order. *Coordination Chemistry Reviews* **2019,** *388*, 107-125.

35. Jiao, J.; Gong, W.; Wu, X.; Yang, S.; Cui, Y. Multivariate crystalline porous materials: Synthesis, property and potential application. *Coordination Chemistry Reviews* **2019,** *385*, 174-190.

36. Chen, Z.; Hanna, S. L.; Redfern, L. R.; Alezi, D.; Islamoglu, T.; Farha, O. K. Reticular chemistry in the rational synthesis of functional zirconium cluster-based MOFs. *Coordination Chemistry Reviews* **2019,** *386*, 32-49.

37. Efome, J. E.; Rana, D.; Matsuura, T.; Lan, C. Q. Insight Studies on Metal-Organic Framework Nanofibrous Membrane Adsorption and Activation for Heavy Metal Ions Removal from Aqueous Solution. *ACS Applied Materials & Interfaces* **2018,** *10*, 18619-18629.

38. Li, Z.-Q.; Yang, J.-C.; Sui, K.-W.; Yin, N. Facile synthesis of metal-organic framework MOF-808 for arsenic removal. *Materials Letters* **2015,** *160*, 412-414.

39. Wang, C.; Liu, X.; Chen, J. P.; Li, K. Superior removal of arsenic from water with zirconium metal-organic framework UiO-66. *Scientific Reports* **2015,** *5*, 16613.

40. Fujie, K.; Ikeda, R.; Otsubo, K.; Yamada, T.; Kitagawa, H. Lithium Ion Diffusion in a Metal–Organic Framework Mediated by an Ionic Liquid. *Chemistry of Materials* **2015,** *27*, 7355-7361.

41. Han, D.-D.; Wang, Z.-Y.; Pan, G.-L.; Gao, X.-P. Metal–Organic-Framework-Based Gel Polymer Electrolyte with Immobilized Anions To Stabilize a Lithium Anode for a Quasi-Solid-State Lithium–Sulfur Battery. *ACS Applied Materials & Interfaces* **2019,** *11*, 18427-18435.

42. Song, C.-L.; Li, G.-H.; Yang, Y.; Hong, X.-J.; Huang, S.; Zheng, Q.-F.; Si, L.-P.; Zhang, M.; Cai, Y.-P. 3D catalytic MOF-based nanocomposite as separator coatings for high-performance Li-S battery. *Chemical Engineering Journal* **2020,** *381*, 122701.

43. Fan, Y.; Niu, Z.; Zhang, F.; Zhang, R.; Zhao, Y.; Lu, G. Suppressing the Shuttle Effect in Lithium–Sulfur Batteries by a UiO-66-Modified Polypropylene Separator. *ACS Omega* **2019,** *4*, 10328-10335.

44. Jiang, J.; Gándara, F.; Zhang, Y.-B.; Na, K.; Yaghi, O. M.; Klemperer, W. G. Superacidity in Sulfated Metal–Organic Framework-808. *Journal of the American Chemical Society* **2014,** *136*, 12844-12847.

45. He, L.; Sun, J.; Wang, X.; Wang, C.; Song, R.; Hao, Y. Facile and effective promotion of β crystalline phase in poly(vinylidene fluoride) via the incorporation of imidazolium ionic liquids. *Polymer International* **2013,** *62*, 638-646.

46. Gören, A.; Mendes, J.; Rodrigues, H. M.; Sousa, R. E.; Oliveira, J.; Hilliou, L.; Costa, C. M.; Silva, M. M.; Lanceros-Méndez, S. High performance screen-printed electrodes prepared by a green solvent approach for lithium-ion batteries. *Journal of Power Sources* **2016,** *334*, 65-77.

47. Miranda, D.; Costa, C. M.; Almeida, A. M.; Lanceros-Méndez, S. Modeling separator membranes physical characteristics for optimized lithium ion battery performance. *Solid State Ionics* **2015,** *278*, 78-84.

48. Luo, X.; Pan, W.; Liu, H.; Gong, J.; Wu, H. Glass fiber fabric mat as the separator for lithium-ion battery with high safety performance. *Ionics* **2015,** *21*, 3135-3139.

49. Thakur, P.; Kool, A.; Bagchi, B.; Das, S.; Nandy, P. Effect of in situ synthesized Fe2O3 and Co3O4 nanoparticles on electroactive β phase crystallization and dielectric properties of poly(vinylidene fluoride) thin films. *Physical Chemistry Chemical Physics* **2015,** *17*, 1368-1378.

50. Lopes, A. C.; Neves, I. C.; Lanceros Mendez, S. Ion Exchange Dependent Electroactive Phase Content and Electrical Properties of Poly(vinylidene fluoride)/Na(M)Y Composites. *The Journal of Physical Chemistry C* **2015,** *119*, 5211-5217.

51. Martins, P.; Lopes, A. C.; Lanceros-Mendez, S. Electroactive phases of poly(vinylidene fluoride): Determination, processing and applications. *Progress in Polymer Science* **2014,** *39*, 683-706.

52. Betz, N.; Le Moël, A.; Balanzat, E.; Ramillon, J. M.; Lamotte, J.; Gallas, J. P.; Jaskierowicz, G. A FTIR study of PVDF irradiated by means of swift heavy ions. *Journal of Polymer Science Part B: Polymer Physics* **1994,** *32*, 1493-1502.

53. Lanceros-Méndez, S.; Mano, J. F.; Costa, A. M.; Schmidt, V. H. FTIR AND DSC STUDIES OF MECHANICALLY DEFORMED β-PVDF FILMS. *Journal of Macromolecular Science, Part B* **2001,** *40*, 517-527.

54. Dias, J. C.; Lopes, A. C.; Magalhães, B.; Botelho, G.; Silva, M. M.; Esperança, J. M. S. S.; Lanceros-Mendez, S. High performance electromechanical actuators based on ionic liquid/poly(vinylidene fluoride). *Polymer Testing* **2015,** *48*, 199-205.

55. Caparros, C.; Lopes, A. C.; Ferdov, S.; Lanceros-Mendez, S. γ-Phase nucleation and electrical response of poly(vinylidene fluoride)/microporous titanosilicates composites. *Materials Chemistry and Physics* **2013,** *138*, 553-558.

56. Mendes, S. F.; Costa, C. M.; Caparros, C.; Sencadas, V.; Lanceros-Méndez, S. Effect of filler size and concentration on the structure and properties of poly(vinylidene fluoride)/BaTiO3 nanocomposites. *Journal of Materials Science* **2012,** *47*, 1378-1388.

57. Reizabal, A.; Gonçalves, R.; Fidalgo-Marijuan, A.; Costa, C. M.; Pérez, L.; Vilas, J.-L.; Lanceros-Mendez, S. Tailoring silk fibroin separator membranes pore size for improving performance of lithium ion batteries. *Journal of Membrane Science* **2020,** *598*, 117678.

58. Chang, B.-Y.; Park, S.-M. Electrochemical Impedance Spectroscopy. *Annual Review of Analytical Chemistry* **2010,** *3*, 207-229.

59. Costa, C. M.; Gomez Ribelles, J. L.; Lanceros-Méndez, S.; Appetecchi, G. B.; Scrosati, B. Poly(vinylidene fluoride)-based, co-polymer separator electrolyte membranes for lithium-ion battery systems. *Journal of Power Sources* **2014,** *245*, 779-786.

60. Appetecchi, G. B.; Romagnoli, P.; Scrosati, B. Composite gel membranes: a new class of improved polymer electrolytes for lithium batteries. *Electrochemistry Communications* **2001,** *3*, 281-284.

61. Nien, Y.-H.; Carey, J. R.; Chen, J.-S. Physical and electrochemical properties of LiFePO4/C composite cathode prepared from various polymer-containing precursors. *Journal of Power Sources* **2009,** *193*, 822-827.

62. Xiao, W.; Zhao, L.; Gong, Y.; Wang, S.; Liu, J.; Yan, C. Preparation of high performance lithium-ion batteries with a separator–cathode assembly. *RSC Advances* **2015,** *5*, 34184-34190.

63. Zheng, Y.; Zheng, S.; Xue, H.; Pang, H. Metal–organic frameworks for lithium–sulfur batteries. *Journal of Materials Chemistry A* **2019,** *7*, 3469-3491.

64. He, Y.; Qiao, Y.; Chang, Z.; Zhou, H. The potential of electrolyte filled MOF membranes as ionic sieves in rechargeable batteries. *Energy & Environmental Science* **2019,** *12*, 2327-2344.

65. Wang, Z.; Wang, S.; Wang, A.; Liu, X.; Chen, J.; Zeng, Q.; Zhang, L.; Liu, W.; Zhang, L. Covalently linked metal–organic framework (MOF)-polymer all-solid-state electrolyte membranes for room temperature high performance lithium batteries. *Journal of Materials Chemistry A* **2018,** *6*, 17227-17234.

66. Hong, X.-J.; Song, C.-L.; Yang, Y.; Tan, H.-C.; Li, G.-H.; Cai, Y.-P.; Wang, H. Cerium Based Metal–Organic Frameworks as an Efficient Separator Coating Catalyzing the Conversion of Polysulfides for High Performance Lithium–Sulfur Batteries. *ACS Nano* **2019,** *13*, 1923-1931.

67. Qiao, Y.; He, Y.; Wu, S.; Jiang, K.; Li, X.; Guo, S.; He, P.; Zhou, H. MOF-Based Separator in an Li–O2 Battery: An Effective Strategy to Restrain the Shuttling of Dual Redox Mediators. *ACS Energy Letters* **2018,** *3*, 463-468.

68. Wu, J.-F.; Guo, X. MOF-derived nanoporous multifunctional fillers enhancing the performances of polymer electrolytes for solid-state lithium batteries. *Journal of Materials Chemistry A* **2019,** *7*, 2653-2659.

69. Guo, J.; Sun, A.; Chen, X.; Wang, C.; Manivannan, A. Cyclability study of silicon–carbon composite anodes for lithium-ion batteries using electrochemical impedance spectroscopy. *Electrochimica Acta* **2011,** *56*, 3981-3987.

70. Zhang, S. S.; Tran, D. T. A simple approach for superior performance of lithium/sulphur batteries modified with a gel polymer electrolyte. *Journal of Materials Chemistry A* **2014,** *2*, 7383-7388.

Table of Contents (TOC)

Metal-Organic Framework (MOF) porous separators enable high rate long term stability cycling of lithium iron phosphate-based batteries. MOF nanoparticles work as templates to modify the macro and mesoporous structure, and surface properties of Polyvinylidene fluoride (PVDF) separators.